

Inverted Pendulum Stabilization of Submarines in Free Positive Buoyancy Ascent

Fotis A. Papoulias¹ and Brian D. McKinley¹

The problem of steady-state vertical ascent of a submarine with excess buoyancy is analyzed. All possible vertical plane solutions are computed and their stability is established in both in-plane and out-of-plane perturbations. Divergence of trajectories, sensitivity of solutions to initial conditions, and stable inverted pendulum configurations are shown to exist for certain ranges of parameters.

Introduction

TRADITIONAL methods of analysis in ship stability concentrate mainly on static stability in roll and directional stability in sway and yaw. Lateral motions in sway and yaw can be strongly coupled with roll, although techniques exist where these can be decoupled. Even with these approximations, roll motion remains a highly nonlinear problem which can be best studied using recently developed techniques in nonlinear dynamics and global analysis (Falzarano et al 1992).

Similar studies can be carried out for submarines with the inclusion of vertical plane stability. Submarines tend to be more stable in the vertical plane due to the nonzero meta-centric height, and the limiting criterion is usually horizontal plane controls fixed stability. The assumptions that are implicit in this analysis scheme are that hydrodynamic forces and moments can be expressed in a series form in terms of the vehicle velocities and accelerations (Abkowitz 1969, Gertler & Hagen 1967), and that the coupling between horizontal and vertical plane motions is fairly weak. For submarines where high amplitude motions may take place in all six degrees-of-freedom, nonlinear interactions between the various modes of motion may become more pronounced. In particular, there is growing evidence of bifurcation phenomena during high-speed maneuvering and emergency ascent scenarios such as recovery from a dive plane jam. In these cases it is no longer true that decoupled linear analysis techniques are sufficient and one is forced to consider the true character of six degrees-of-freedom motions. In this paper we study the coupled steady state and motion stability analysis problem of a submarine during a free positive buoyancy ascent. This poses significant differences with respect to the neutrally buoyant case and may give rise to certain pathological situations where counter-intuitive stable motions develop. The problem has received limited attention in the past, mainly by Booth (1977) where the response was distinguished into either a nearly vertical ascent or a predominantly forward motion. It is found here that this distinction is not always meaningful as a result of the many parameters that affect the problem. As a first step into a more critical examination, criteria are developed which allow for steady state vertical plane ascent. Stability analysis is performed for both vertical and horizontal plane motions. A divergent type of instability is observed for certain ranges

of parameters, as well as an inverted pendulum stabilization which is accompanied by an extreme sensitivity of the response to the initial conditions. Physically, this inverted pendulum stabilization corresponds to a vehicle which remains dynamically stable in a keel-up configuration, even though such a position is statically unstable! This inverted pendulum stabilization occurs in the absence of time-dependent external excitation, so that it is of a different nature than vibrational stabilization. Numerical integration studies are performed which indicate that the inverted pendulum stabilization persists under continuously acting disturbances. It is argued that the phenomenon is due to coupling between roll and lateral (sway and yaw) motions. All computations in this work are performed for the Swimmer Delivery Vehicle (SDV), a 17.4 ft vehicle, for which a complete set of hydrodynamic and geometric properties is available (Smith et al 1978). Unless specified otherwise, all results in this work are presented in dimensional form, linear dimensions in feet, velocities in feet per second, angular deflections in degrees, and time in seconds.

1. Problem formulation

In this section we present the vehicle dynamic equations of motion along with the kinematic relations. The system is then placed in state space form and some general topological properties of solutions are discussed.

Equations of motion

The six-degrees-of-freedom equations of motion for a submarine in surge, sway, heave, roll, pitch, and yaw, respectively, are

$$m[\dot{u} - vr + wq - x_G(q^2 + r^2) + y_G(pq - \dot{r}) + z_G(pr + \dot{q})] = X_H + X_W + X_C \quad (1)$$

$$m[\dot{v} + ur - wp + x_G(pq + \dot{r}) - y_G(p^2 + r^2) + z_G(qr - \dot{p})] = Y_H + Y_W + Y_C \quad (2)$$

$$m[\dot{w} - uq + vp + x_G(pr - \dot{q}) + y_G(qr + \dot{p}) - z_G(p^2 + q^2)] = Z_H + Z_W + Z_C \quad (3)$$

$$I_x \dot{p} + (I_z - I_y)qr + I_{xy}(pr - \dot{q}) - I_{yz}(q^2 - r^2) - I_{xz}(pq + \dot{r}) + m[y_G(\dot{w} - uq + vp) - z_G(\dot{v} + ur - wp)] = K_H + K_W + K_C \quad (4)$$

$$I_y \dot{q} + (I_x - I_z)pr - I_{xy}(qr + \dot{p}) + I_{yz}(pq - \dot{r}) + I_{xz}(p^2 - r^2)$$

¹Assistant professor and lieutenant, U.S. Navy, respectively, Department of Mechanical Engineering, Naval Postgraduate School, Monterey, California.

Manuscript received at SNAME headquarters June 18, 1992; revised manuscript received November 16, 1992.

$$-m[x_G(\dot{w} - uq + vp) - z_G(\dot{u} - vr + wq)] \\ = M_H + M_W + M_C \quad (5)$$

$$I_z \dot{r} + (I_y - I_x)pq - I_{xy}(p^2 - q^2) - I_{yz}(pr + \dot{q}) + I_{xz}(qr - \dot{p}) \\ + m[x_G(\dot{v} + ur - wp) - y_G(\dot{u} - vr + wq)] \\ = N_H + N_W + N_C \quad (6)$$

where the left-hand sides represent inertial forces and moments (Newton's Law) and the right-hand sides model the external forces. Subscript *H* reflects hydrodynamic contributions, *W* buoyancy and weight effects, *C* forces arising from control surface (rudders, dive planes, and bow planes) actions, and the rest of the symbols are based on standard notation and explained in the Nomenclature. The hydrodynamic radiation and viscous forces are expressed as

$$X_H = X_{pp}p^2 + X_{qq}q^2 + X_{rr}r^2 + X_{pr}pr + X_u\dot{u} + X_{wq}wq \\ + X_{vp}vp + X_{vr}vr + X_{vv}v^2 + X_{uw}uw^2 - C_{D0}u^2 \quad (7)$$

$$Y_H = Y_{\dot{p}}\dot{p} + Y_{\dot{r}}\dot{r} + Y_{pq}pq + Y_{qr}qr + Y_v\dot{v} \\ + Y_{\dot{p}}up + Y_{ur}ur + Y_{vq}vq + Y_{wp}wp + Y_{wr}wr \\ + Y_{vu}uv + Y_{vw}vw - \frac{1}{2}\rho \int [C_{Dy}h(x)(v + xr)^2 \\ + C_{Dz}b(x)(w - xq)^2] \frac{(v + xr)}{U_{cf}(x)} dx \quad (8)$$

$$Z_H = Z_{\dot{q}}\dot{q} + Z_{pp}p^2 + Z_{pr}pr + Z_{rr}r^2 + Z_{w\dot{w}}\dot{w} + Z_{qu}uq \\ + Z_{vp}vp + Z_{vr}vr + Z_{uw}uw + Z_{vv}v^2 - \frac{1}{2}\rho \int [C_{Dy}h(x)(v \\ + xr)^2 + C_{Dz}b(x)(w - xq)^2] \frac{(w - xq)}{U_{cf}(x)} dx \quad (9)$$

$$K_H = K_{\dot{p}}\dot{p} + K_{\dot{r}}\dot{r} + K_{pq}pq + K_{qr}qr + K_v\dot{v} + K_pup \\ + K_rur + K_{vq}vq + K_{wp}wp + K_{wr}wr + K_vuv + K_{vw}vw \quad (10)$$

$$M_H = M_{\dot{q}}\dot{q} + M_{pp}p^2 + M_{pr}pr + M_{rr}r^2 + M_w\dot{w} + M_{qu}uq \\ + M_{vp}vp + M_{vr}vr + M_{uw}uw + M_{vv}v^2 + \frac{1}{2}\rho \int \\ [C_{Dy}h(x)(v + xr)^2 + C_{Dz}b(x)(w - xq)^2] \frac{(w - xq)}{U_{cf}(x)} x dx \quad (11)$$

$$N_H = N_{\dot{p}}\dot{p} + N_{\dot{r}}\dot{r} + N_{pq}pq + N_{qr}qr + N_v\dot{v} \\ + N_{\dot{p}}up + N_{ur}ur + N_{vq}vq + N_{wp}wp + N_{wr}wr + N_{vu}uv \\ + N_{vw}vw - \frac{1}{2}\rho \int [C_{Dy}h(x)(v + xr)^2 \\ + C_{Dz}b(x)(w - xq)^2] \frac{(v + xr)}{U_{cf}(x)} x dx \quad (12)$$

These are given in the customary form of series expansions in terms of the hydrodynamic coefficients and cross flow integral terms which are integrated over the entire length of the body and represent quadratic drag forces. The cross-flow velocity U_{cf} is

$$U_{cf} = [(v + xr)^2 + (w - xq)^2]^{1/2} \quad (13)$$

Hydrostatic restoring forces and moments are due to the vehicle weight *W* and buoyancy *B*, and are given by

$$X_W = -(W - B) \sin \theta \quad (14)$$

$$Y_W = (W - B) \cos \theta \sin \phi \quad (15)$$

$$Z_W = (W - B) \cos \theta \cos \phi \quad (16)$$

$$K_W = (y_G W - y_B B) \cos \theta \cos \phi \\ - (z_G W - z_B B) \cos \theta \sin \phi \quad (17)$$

$$M_W = -(x_G W - x_B B) \cos \theta \cos \phi - (z_G W - z_B B) \sin \theta \quad (18)$$

$$N_W = (x_G W - x_B B) \cos \theta \sin \phi + (y_G W - y_B B) \sin \theta \quad (19)$$

Forces and moments due to control surface deflections are reflected as added drag in surge, while in sway, heave, pitch,

Nomenclature

A_H = linearized horizontal plane system matrix
 A_V = linearized vertical plane system matrix
B = vehicle buoyancy
 B_H = mass matrix in horizontal plane
 B_V = mass matrix in vertical plane
 C_{Dy} = drag coefficient in sway
 C_{Dz} = drag coefficient in heave
e = combined degree of stability
 e_H = degree of stability in horizontal plane
 e_V = degree of stability in vertical plane
K = roll moment
L = vehicle length
M = pitch moment

N = yaw moment
p = roll angular velocity
q = pitch angular velocity
r = yaw angular velocity
u = surge translational velocity
v = sway translational velocity
w = heave translational velocity
W = vehicle weight
X = surge force
 x_H = horizontal plane state variables vector
 $x_G(x_B)$ = x-coordinate of center of gravity (buoyancy)
 x_{GB} = LCG/LCB separation
 x_V = vertical plane state variables vector

Y = sway force
Z = heave force
 $z_G(z_B)$ = z-coordinate of center of gravity (buoyancy)
 z_{GB} = metacentric height

Greek symbols

δ_b = bow plane angle
 δB = excess buoyancy
 δ_r = rudder angle
 δ_s = dive plane angle
 λ_H = horizontal plane eigenvalue
 λ_V = vertical plane eigenvalue
 θ = pitch angle
 ϕ = roll angle
 ψ = yaw angle

and yaw they are directly proportional to the control surface deflection

$$X_C = uq(X_{q\delta_s}\delta_s + X_{q\delta_b}\delta_b) + X_{r\delta_r}ur\delta_r + X_{v\delta_r}uv\delta_r + uw(X_{w\delta_s}\delta_s + X_{w\delta_b}\delta_b) + u^2(X_{\delta_s}\delta_s^2 + X_{\delta_b}\delta_b^2 + X_{\delta_r}\delta_r^2) \quad (20)$$

$$Y_C = Y_{\delta_r}u^2\delta_r \quad (21)$$

$$Z_C = u^2(Z_{\delta_s}\delta_s + Z_{\delta_b}\delta_b) \quad (22)$$

$$K_C = 0 \quad (23)$$

$$M_C = u^2(M_{\delta_s}\delta_s + M_{\delta_b}\delta_b) \quad (24)$$

$$N_C = N_{\delta_r}u^2\delta_r \quad (25)$$

Usually, control surface deflections are kept intentionally small, and the linearity assumption in (21), (22), (24), and (25) remains valid. Unlike the surface ship case, the roll moment K_C is zero for a submersible since the rudder is centered with the vehicle centerplane. The hydrodynamic coefficients in equations (7–12) are functions of the frequency of motion, or what amounts to the same thing, functions of the maneuver at hand. In this paper we study slowly varying reference motions and we can, therefore, assume that they remain constant and equal to their zero frequency limit (Abkowitz 1969). This has been shown to result in negligible errors compared to more accurate simulations incorporating the time history of motion through convolution integrals (Tinker 1978). It should be emphasized, though, that the constant coefficient assumption would break down in studies related to fast motions under the action of first-order wave forces in the case of a nearly surfaced submarine. Another important assumption in this study is that they are assumed to be constant throughout the range of vehicle angle of attack. Ordinary maneuvering models are usually validated for angles of attack between ± 15 deg. For higher angles of attack the cross-flow drag terms C_{D_y} and C_{D_z} dominate the response and they are functions of the side slip angle and angle of attack. Considering them to be constant does not, however, alter significantly the behavioral characteristics and qualitative bifurcation results that are derived. Similarly, C_{D_y} and C_{D_z} are functions of speed due to the Reynolds number effect on cross-flow drag (Humphreys 1990). This is more pronounced in small-size, unmanned, untethered vehicles, whereas for submarines the cross-flow drag terms remain relatively constant over the entire speed range. The methods developed in this work can easily accommodate angle of attack and speed dependence, if desired.

To complete the model, we need the expressions for the Euler angles rates of change

$$\dot{\phi} = p + q \sin \phi \tan \theta + r \cos \phi \tan \theta \quad (26)$$

$$\dot{\theta} = q \cos \phi - r \sin \phi \quad (27)$$

$$\dot{\psi} = q \frac{\sin \phi}{\cos \theta} + r \frac{\cos \phi}{\cos \theta} \quad (28)$$

Notice that the transformation matrix embedded in (26–28) is singular for a pitch angle of $\theta = \pm 90$ deg. In such a case, the kinematic equations can be described by two Euler angle representations with different singularities (Fossen 1991). As an alternative to the Euler angle representation, one could employ a four-parameter method based on the Cayley-Klein parameters (Kane et al 1983).

Finally, it is assumed that propulsion is inoperative and the propeller is rotating freely. For this reason, propulsive forces are not included in equations (1–6). The driving

mechanism for the vehicle is its excess buoyancy, $B - W > 0$. The problem then is to assess the asymptotic dynamic characteristics of the system during this condition of free positive buoyancy ascent.

State space representation

The model presented in the previous subsection can be written in its Cauchy standard form by selecting as state variables

$$x_1 = u, x_2 = v, x_3 = w, x_4 = p, x_5 = q, x_6 = r, x_7 = \phi, x_8 = \theta \quad (29)$$

where the first six describe the system motion and the last two its geometry. Notice that the yaw angle ψ does not affect directly the equations of motion and is, therefore, not included in (29). Angle ψ can be computed from (28) once the time histories of the state variables (29) have been obtained.

In a compact vector form the state equations can be written as

$$\dot{\mathbf{x}} = \mathbf{f}(\mathbf{x}), \mathbf{f}: M \rightarrow TM \quad (30)$$

where bold face indicates a vector, M is the eight-dimensional smooth manifold $R^6 \times S^1 \times S^1$ where the circular component $S^1 = R$ (modulo 2π) reflects the periodicity of the vector field \mathbf{f} in x_5, x_6 , and TM is the tangent bundle of M . Local analysis of properties of the state equations (30) can be performed in the Euclidean space R^8 which is locally homeomorphic to M . With $x \in M$ it can be easily seen that $\mathbf{f} \in C^1$ and thus \mathbf{f} is locally Lipschitz continuous in \mathbf{x} . Therefore, (30) has a unique solution over some time interval and this solution depends continuously on the initial state. Since we are working on a noncompact state space, however, global existence or boundedness of solutions cannot be established without further investigation (Guckenheimer & Holmes 1983). In our case this can be easily verified by letting $x_i \rightarrow \infty, i = 1, \dots, 6$ and noting that the corresponding right-hand sides of (30) are all negative since they represent damping due to viscous and radiation effects. Therefore, x_i are negative and x_i are bounded. Finally, the last two components of vector \mathbf{x} , x_7 and x_8 are defined on the torus $S^1 \times S^1$ which is a compact two-manifold, and x_7, x_8 cannot escape for any $t \in R_+$.

2. Equilibrium solutions

The first step in analyzing local properties of solutions of (30) is to establish the equilibrium solutions where the vector field \mathbf{f} vanishes. Stability analysis of these equilibrium solutions is the subject of Section 3.

Steady-state conditions

Steady-state conditions are achieved when the submersible reaches constant linear and angular velocities which must assume finite values following the discussion of the State space representation section. Therefore, the body-fixed linear accelerations $(\dot{u}, \dot{v}, \dot{w})$ and the body-fixed angular accelerations $(\dot{p}, \dot{q}, \dot{r})$ will be zero. Likewise, the vehicle will have reached constant angles of roll ϕ and pitch θ , making the derivatives $\dot{\phi} = \dot{\theta} = 0$. These steady state solutions can be computed by solving the system of eight coupled nonlinear algebraic equations

$$\mathbf{f}(\bar{\mathbf{x}}) = \mathbf{0} \quad (31)$$

where the overbar denotes an equilibrium solution. Substituting $\dot{\phi} = \dot{\theta} = 0$ in equations (26–28) we can get the steady-state values of the angular velocities as

$$\begin{aligned} p &= -\dot{\psi} \sin \theta \\ q &= \dot{\psi} \sin \phi \cos \theta \\ r &= \dot{\psi} \cos \phi \cos \theta \end{aligned} \quad (32)$$

where the overbar has been dropped from the notation for convenience. Substituting (32) into (31) then yields a reduced system of six equations to be solved for the steady state values of u , v , w , ϕ , θ , and ψ . This is a highly nonlinear system of equations and it may exhibit solution branching and/or multiple solutions (Golubitsky & Schaeffer 1985). In order to gain some insight into the problem we make the additional assumption $\psi = 0$ at steady state: This forces a constant yaw angle at equilibrium and as a result it restricts the equilibrium set in the vertical plane.

Vertical plane analysis

We define the amount of excess buoyancy as $\delta B = B - W$, the longitudinal center of buoyancy/gravity separation $x_{GB} = x_G - x_B$, the lateral center of buoyancy/gravity separation $y_{GB} = y_G - y_B$, and the metacentric height $z_{GB} = z_G - z_B$. Using these definitions, the expression $(z_G W - z_B B)$ may be written as $(z_{GB} W - z_B \delta B)$. Similarly, $x_G W - x_B B = x_{GB} W - x_B \delta B$ and $y_G W - y_B B = y_{GB} W - y_B \delta B$. Since $\psi = 0$, equations (32) result in $p = q = r = 0$, and the complete steady state characterization is obtained from equations (1–6) which take the form

$$X_{vv}v^2 + X_{ww}w^2 - C_{D0}u^2 + X_{v\delta_r}v\delta_r + uw(X_{w\delta_s}\delta_s + X_{w\delta_b}\delta_b) + u^2(X_{\delta_s\delta_s}\delta_s^2 + X_{\delta_b\delta_b}\delta_b^2 + X_{\delta_s\delta_r}\delta_r^2) + \delta B \sin \theta = 0 \quad (33)$$

$$Y_v uv + Y_{vw}vw - \int [C_{Dv}h(x)v^2 + C_{Dz}b(x)w^2] \frac{v}{U_{cf}} dx + Y_{\delta_r}u^2\delta_r - \delta B \cos \theta \sin \phi = 0 \quad (34)$$

$$Z_w uw + Z_{vv}v^2 - \int [C_{Dv}h(x)v^2 + C_{Dz}b(x)w^2] \frac{w}{U_{cf}} dx + u^2(Z_{\delta_s}\delta_s + Z_{\delta_b}\delta_b) - \delta B \cos \theta \cos \phi = 0 \quad (35)$$

$$K_v uv + K_{vw}vw + (y_{GB}W - y_B\delta B) \cos \theta \cos \phi - (z_{GB}W - z_B\delta B) \cos \theta \sin \phi = 0 \quad (36)$$

$$M_w uw + M_{vv}v^2 - \int [C_{Dv}h(x)v^2 + C_{Dz}b(x)w^2] \frac{w}{U_{cf}} x dx + u^2(M_{\delta_s}\delta_s + M_{\delta_b}\delta_b) - (x_{GB}W - x_B\delta B) \cos \theta \cos \phi - (z_{GB}W - z_B\delta B) \sin \theta = 0 \quad (37)$$

$$N_v uv + N_{vw}vw - \int [C_{Dv}h(x)v^2 + C_{Dz}b(x)w^2] \frac{v}{U_{cf}} x dx + N_{\delta_r}u^2\delta_r + (x_{GB}W - x_B\delta B) \cos \theta \sin \phi + (y_{GB}W - y_B\delta B) \sin \theta = 0 \quad (38)$$

where the drag coefficients C_{Dv} , C_{Dz} have been redefined to absorb the 0.5ρ term for convenience.

The six equations (33–38) have only five unknowns, namely u , v , w , ϕ , and θ . Therefore, a solution, in general, does not exist. This is because of the previous condition $\psi = 0$ which restricts motion in the dive plane. This restriction requires that $v = \sin \phi = 0$ as well. Then the sway equation (34) requires that

$$\delta_r = 0 \quad (39)$$

and the roll equation (36) that

$$y_{GB}W - y_B\delta B = 0 \quad (40)$$

while the yaw equation (38) does not furnish any additional requirements. The last two conditions (39), or rudder at zero, and (40), or center of gravity/buoyancy "symmetry" with re-

spect to the centerplane, are the two necessary conditions to allow motion in the vertical plane only.

The system which describes steady-state solutions in the vertical plane is then

$$X_{ww}w^2 - C_{D0}u^2 + uw(X_{w\delta_s}\delta_s + X_{w\delta_b}\delta_b) + u^2(X_{\delta_s\delta_s}\delta_s^2 + X_{\delta_b\delta_b}\delta_b^2) + \delta B \sin \theta = 0 \quad (41)$$

$$Z_w uw + u^2(Z_{\delta_s} + Z_{\delta_b}\delta_b) - C_{Dz}w|w|A_w - \delta B \cos \theta \cos \phi = 0 \quad (42)$$

$$M_w uw + u^2(M_{\delta_s}\delta_s + M_{\delta_b}\delta_b) - C_{Dz}w|x_A A_w - (x_{GB}W - x_B\delta B) \cos \theta \cos \phi - (z_{GB}W - z_B\delta B) \sin \theta = 0 \quad (43)$$

where we have defined

$$A_w = \int (b(x)dx), \quad x_A = \frac{1}{A_w} \int xb(x)dx \quad (44)$$

and the drag coefficient C_{Dz} is assumed to be constant throughout the length of the body. In equations (42) and (43), $\cos \phi$ can take the values ± 1 only because for motion to be restricted in the vertical plane the roll angle ϕ is either zero or π . If (41) and (42) are solved for $\sin \theta$ and $\cos \theta$, respectively, and the result is substituted in (43) we get

$$w|w| + aw^2 + buw + cu^2 = 0 \quad (45)$$

where

$$a = \frac{p_z X_{ww}}{C_{Dz} A_w (p_x + x_A \delta B)}$$

$$b = \frac{M_w \delta B - p_x Z_w + p_z (X_{w\delta_s} \delta_s + X_{w\delta_b} \delta_b)}{C_{Dz} A_w (p_x + x_A \delta B)}$$

$$c = \frac{\delta B (M_{\delta_s} \delta_s + M_{\delta_b} \delta_b) + p_z (X_{\delta_s\delta_s} \delta_s^2 + X_{\delta_b\delta_b} \delta_b^2 - C_{D0}) + p_x (Z_{\delta_s} \delta_s + Z_{\delta_b} \delta_b)}{C_{Dz} A_w (p_x + x_A \delta B)} \quad (46)$$

and we have introduced the parameters

$$p_x = x_{GB}W - x_B\delta B \quad (47)$$

$$p_z = z_{GB}W - z_B\delta B \quad (48)$$

Following Booth (1977) we divide (45) by u^2 and we get a single equation in $x = w/u$, the nondimensional steady state heave velocity, as

$$\pm x|x| + ax^2 + bx + c = 0 \quad (49)$$

where the plus sign is used when u is positive, and the minus sign when u is negative. The pitch angle θ can then be evaluated from

$$\tan \theta = \frac{X_{\delta_s\delta_s}\delta_s^2 + X_{\delta_b\delta_b}\delta_b^2 - C_{D0} + x(X_{w\delta_s}\delta_s + X_{w\delta_b}\delta_b) + X_{ww}x^2}{[\pm C_{Dz}A_w x|x| - Z_w x - (Z_{\delta_s}\delta_s + Z_{\delta_b}\delta_b)] \cos \phi} \quad (50)$$

where the same agreement concerning the \pm signs as in (49) is understood. The steady state velocity u is then computed from (41) as

$$u^2 = \frac{\delta B \sin \theta}{C_{D0} - X_{ww}x^2 - (X_{\delta_s\delta_s}\delta_s^2 + X_{\delta_b\delta_b}\delta_b^2) - (X_{w\delta_s}\delta_s + X_{w\delta_b}\delta_b)x} \quad (51)$$

With these equations, the steady state vehicle response in the vertical plane is completely determined.

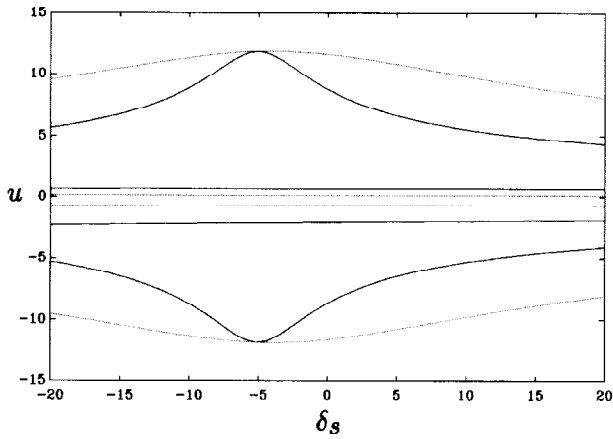


Fig. 1 Steady-state vertical plane solutions for surge velocity for $x_{GB} = -1\%L$ (solid line) and $x_{GB} = +1\%L$ (dotted line)

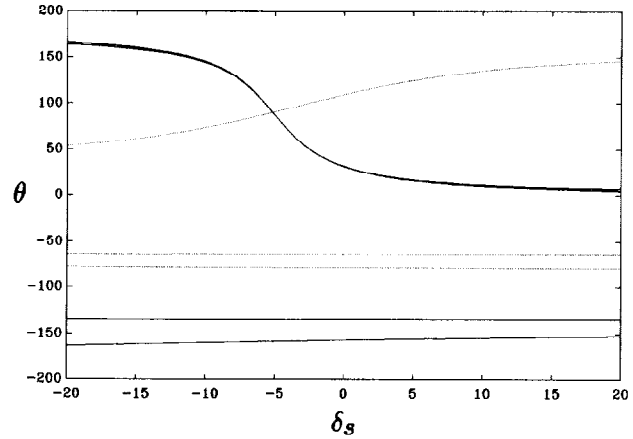


Fig. 3 Steady-state vertical plane solutions for pitch angle $x_{GB} = -1\%L$ (solid line) and $x_{GB} = +1\%L$ (dotted line)

Typical results

Figures 1 through 3 show typical steady state solutions for surge velocity u , in ft/sec, heave velocity w , in ft/sec, and pitch angle θ , in deg, as a function of dive plane angle δ_s , in deg. Two cases are shown which are distinguished by the LCB/LCG separation: the first case, in solid curves, is for $x_{GB} = -1\%$ of the vehicle length L , and the second case, in dotted curves, is for $x_{GB} = +1\%L$. The following parameters were kept the same for both cases: excess buoyancy $\delta B = 2\%$ of the vehicle weight W , deflection of bow planes $\delta_b = 0$, location of horizontal and vertical centers of buoyancy $x_B = z_B = 0$, and location of vertical center of gravity $z_{GB} = 0.1$ feet.

As is evident from equation (49), four solutions exist in general. For two of the solutions, the magnitudes of the surge velocities are large while the magnitudes of the corresponding heave velocities are relatively small. This has been described as "predominantly forward motion" (Booth 1977). The other two solutions have small surge velocity magnitudes and large heave velocity magnitudes, and they are termed as "nearly vertical ascents." This distinction is for zero dive plane angle only, while for nonzero plane deflections all four solutions have similar magnitudes. It should be noted that

in all cases the vehicle steady state solution represents physically ascent towards the surface; the positive or negative nature of the velocities are associated with the value of pitch angle. Positive surge velocity is forward, negative heave is up, and positive pitch angle is bow up. It can be seen from the figures that positive heave velocities are associated with pitch angles greater than 90 deg, that is, the vehicle would be ascending in a keel-up orientation. All solutions shown in the figures correspond to roll angle $\phi = 0$. When $\phi = 180$ deg, u and w remain the same while the steady state pitch angle θ is the supplement of the $\phi = 0$ solution, as can be seen from equation (50). This introduces four more solutions in θ , as shown in Fig. 4 for the $x_{GB} = -1\%L$ case. This demonstrates that a solution for θ less than 90 deg is always present.

Although the steady state analysis of this section computes all possible solutions in the vertical plane, it gives no indication as to which of the solutions are stable, if any. Physically, one would expect that solutions in $\theta > 0.5\pi$ would be unstable since they correspond to an inverted pendulum case with an equivalent negative metacentric height. This problem of stability analysis is the subject of the following section.

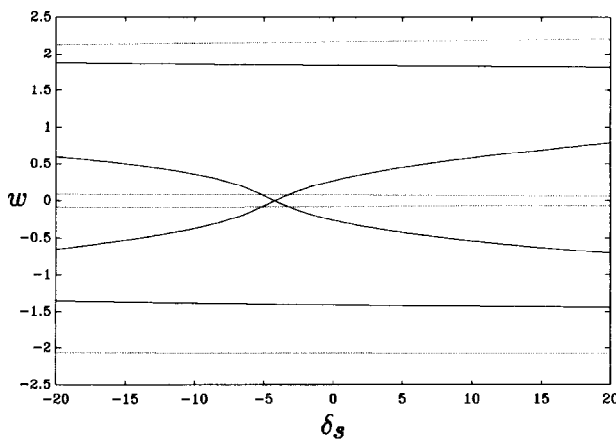


Fig. 2 Steady-state vertical plane solutions for heave velocity for $x_{GB} = -1\%L$ (solid line) and $x_{GB} = +1\%L$ (dotted line)

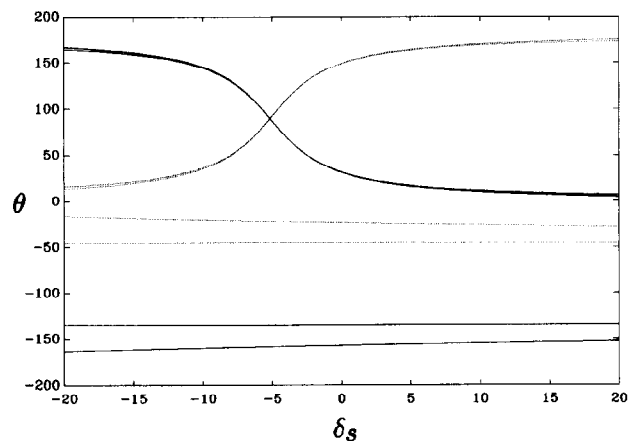


Fig. 4 Steady-state pitch angle for $\phi = 0$ (solid line) and $\phi = \pi$ (dotted line)

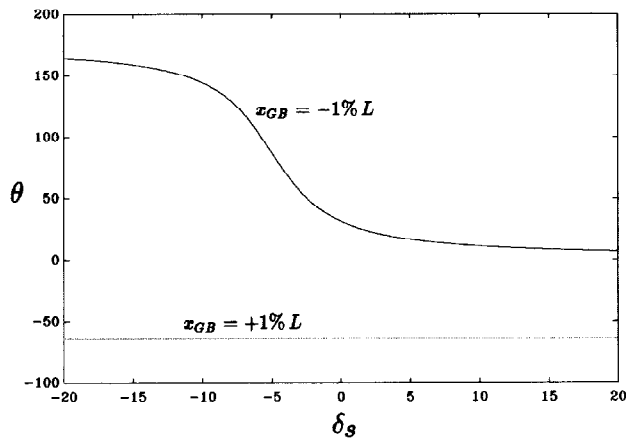


Fig. 5 Stable vertical plane pitch angle

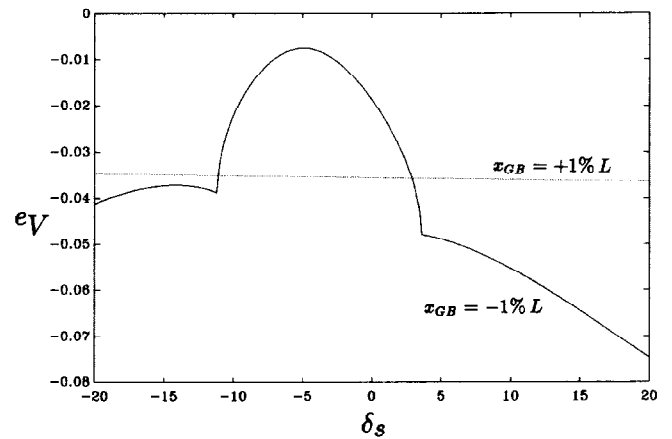


Fig. 6 Degree of stability in vertical plane

3. Stability of motion

Dynamic stability of motion of (30) around its nominal solution (29) can be established by Lyapunov's linearization method (Hahn 1967). Local perturbation of (30) in the neighborhood of $\bar{\mathbf{x}}$ produces a linear system

$$\dot{\mathbf{x}} = \mathbf{A}(\mathbf{x} - \bar{\mathbf{x}})$$

where \mathbf{A} is the Jacobian matrix of first partial derivatives of $\mathbf{f}(\mathbf{x})$ with respect to \mathbf{x} evaluated at $\bar{\mathbf{x}}$. Provided all eigenvalues of \mathbf{A} have negative real parts, $\bar{\mathbf{x}}$ is asymptotically stable, and if at least one eigenvalue of \mathbf{A} is positive $\bar{\mathbf{x}}$ is unstable. Motion stability is assessed in this section first by analyzing the vertical plane dynamics and then proceeding to six degrees-of-freedom.

Vertical plane

In order to establish stability properties in the vertical plane we set all state variables equal to zero except for u , w , q , and θ . In this way we get a system of four first-order nonlinear coupled differential equations, and upon linearization we get the linear system

$$\mathbf{B}_V \dot{\mathbf{x}}_V = \mathbf{A}_V \mathbf{x}_V \quad (52)$$

where $\mathbf{x}_V = [u, w, q, \theta]$ is the state vector in the vertical plane, and the elements of matrices \mathbf{A}_V , \mathbf{B}_V are presented in the Appendix. Vertical plane stability can be established based on the solutions to the generalized eigenvalue problem

$$|\mathbf{A}_V - \lambda_V \mathbf{B}_V| = 0 \quad (53)$$

where λ_V denotes a vertical plane eigenvalue.

Typical results are shown in Fig. 5 for the two cases $x_{GB} = \pm 1\%L$ analyzed in Figs. 1-4. It can be seen that of the four solutions, one is in general stable. Depending on the value of x_{GB} and δ_s , this stable solution in θ may exceed 90 deg. The degree of stability in the vertical plane, e_V , is defined as the largest real part of all eigenvalues λ_V and is shown in Fig. 6. This represents a certain measure of the smallest rate of exponential convergence to the nominal value of solutions when negative, and the largest rate of exponential divergence of solutions when positive.

In the last two figures and all similar figures that follow, we present the stable steady state solutions in θ (in deg) versus the dive plane angle δ_s (in deg) for $\phi = 0$. The reason is that the stability properties of the supplement solution $\pi - \theta$ for $\phi = \pi$ are identical. To see this consider the \mathbf{A}_V matrix

in (52). Based on the expressions given in the Appendix, \mathbf{A}_V takes the form

$$\begin{bmatrix} a_{11} & a_{12} & a_{13} & a_{14}\epsilon \\ a_{21} & a_{22} & a_{23} & a_{24}\epsilon \\ a_{31} & a_{32} & a_{33} & a_{34}\epsilon \\ 0 & 0 & \epsilon & 0 \end{bmatrix}$$

where $\epsilon = +1$ for $(\theta, \phi) = (\bar{\theta}, 0)$ and $\epsilon = -1$ for $(\theta, \phi) = (\pi - \bar{\theta}, \pi)$. It can be easily seen that the characteristic equation of \mathbf{A}_V is even in ϵ and since \mathbf{B}_V is constant, it follows that the eigenvalues λ_V remain the same for $\epsilon = \pm 1$. This means that a stable "inverted pendulum" solution in the vertical plane exists always.

Six degrees of freedom

The previous analysis was valid for motions restricted in the vertical plane. In order to evaluate the complete motion stability properties we proceed with linearization of the full 8×8 system (30). If we rearrange the state variables (29) in the form

$$\mathbf{x} = [\mathbf{x}_V, \mathbf{x}_H]$$

where $\mathbf{x}_V = [u, w, q, \theta]$ refers to vertical plane, and $\mathbf{x}_H = [p, \phi, v, r]$ to horizontal plane variables, we get a linearized system in the form

$$\begin{bmatrix} \mathbf{B}_V & \mathbf{0} \\ \mathbf{0} & \mathbf{B}_H \end{bmatrix} \begin{bmatrix} \dot{\mathbf{x}}_V \\ \dot{\mathbf{x}}_H \end{bmatrix} = \begin{bmatrix} \mathbf{A}_V & \mathbf{0} \\ \mathbf{0} & \mathbf{A}_H \end{bmatrix} \begin{bmatrix} \mathbf{x}_V \\ \mathbf{x}_H \end{bmatrix}$$

in other words, within linearity, the horizontal and vertical plane dynamics are decoupled. The vertical plane eigenvalues remain the same as in (53), while the horizontal plane eigenvalues are computed from

$$|\mathbf{A}_H - \lambda_H \mathbf{B}_H| = 0 \quad (54)$$

where the elements of \mathbf{A}_H , \mathbf{B}_H are given in the Appendix. The six-degrees-of-freedom stability indices are then simply the union of λ_V and λ_H .

The degree of stability e_H in the horizontal plane is shown in Fig. 7 along with the combined degree of stability $e = \max(e_V, e_H)$ in Fig. 8 for the same two cases depicted in Figs. 5 and 6. It can be seen that the $x_{GB} = +1\%L$ case is stable regardless of the value of δ while for $x_{GB} = -1\%L$ there ex-

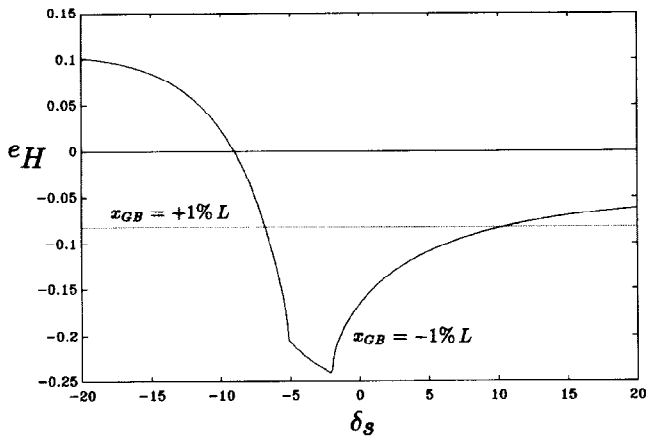


Fig. 7 Degree of stability in horizontal plane

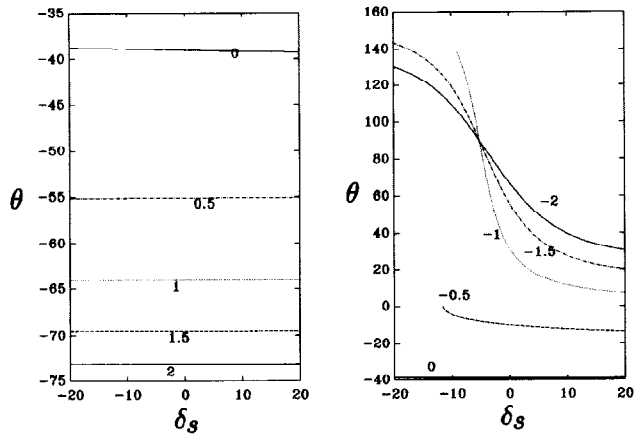


Fig. 9 Stable pitch angle solutions for variations in x_{GB} (in %L)

ists a value of δ_s which renders the nominal point unstable. This is a horizontal plane instability and as was observed in all numerical experiments in this work, horizontal plane stability dominated the overall six-degrees-of-freedom stability of the system. This is generally true for submarines where unless the forward speed is very high, the vehicle is significantly more stable in vertical plane than horizontal plane motions. Figures 5 and 8 demonstrate that the inverted pendulum stabilization is indeed possible in six-degrees-of-freedom motions. It should be mentioned that the magnitudes of the degree of stability indices shown in Figs. 6–8 are of the same order of magnitude as the stability indices for the neutrally buoyant vehicle (McKinley 1991).

The entries of matrix \mathbf{A}_H are identical for $(\theta, \phi) = (\pi - \bar{\theta}, \pi)$ as for $(\theta, \phi) = (\bar{\theta}, 0)$ so that their stability properties are the same. As can be seen from Fig. 4, an inverted pendulum solution exists and is dynamically stable for positive dive plane deflections as well. It follows that, in general, two vertical plane solutions are stable in all six-degrees-of-freedom motions and one of these solutions resembles an inverted pendulum stable ascent.

Results and discussion

A systematic sensitivity analysis is performed here in order to evaluate the influence of several parameters on sys-

tem response. The dynamic stability analysis included in this subsection considers stability in all six degrees of freedom. As was mentioned previously, horizontal plane stability generally dictates overall vehicle stability.

Figure 9 shows how changing the longitudinal center of gravity, x_{GB} , affects the dynamic response of the vehicle. For these cases, the amount of excess buoyancy, δB , is 2% of weight, W , the bow plane deflection angle, δ_b , is zero, the metacentric height, z_{GB} , is 0.1 ft, and the longitudinal and vertical centers of buoyancy are both zero. The parameter x_{GB} parametrizes the curves in the figure and is varied from -2 to +2% of vehicle length. It can be seen that when x_{GB} is positive; i.e., center of gravity forward of center of buoyancy, there are stable solutions for the full range of dive plane angles, and these occur in the form of nearly vertical ascents. As the center of gravity moves aft of the center of buoyancy, $x_{GB} < 0$, stable solutions begin to take the form of predominantly forward motions and exist only for a limited range of δ .

Figure 10 shows the stable pitch angles versus δ_s with the amount of excess buoyancy, δB , as a parameter (in %W). For all these cases $\delta_b = 0$, $x_{GB} = -0.5\%L$, $z_{GB} = 0.1$ ft, and $x_B = z_B = 0$. As δB is varied, the character of solutions changes between nearly vertical ascents and predominantly forward motions. For high values of δB , no stable solutions in the vertical plane exist throughout the range of δ_s .

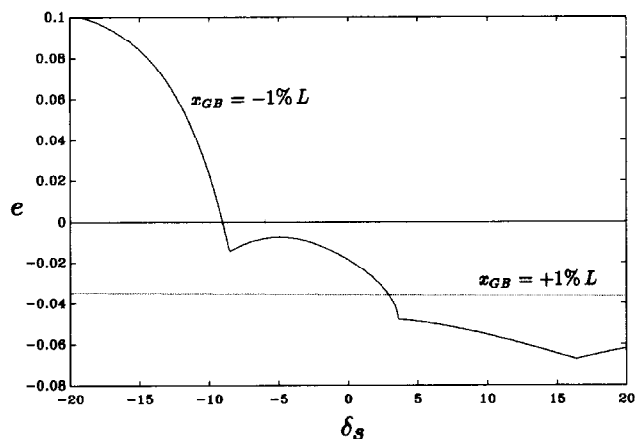


Fig. 8 Combined degree of stability in six degrees of freedom

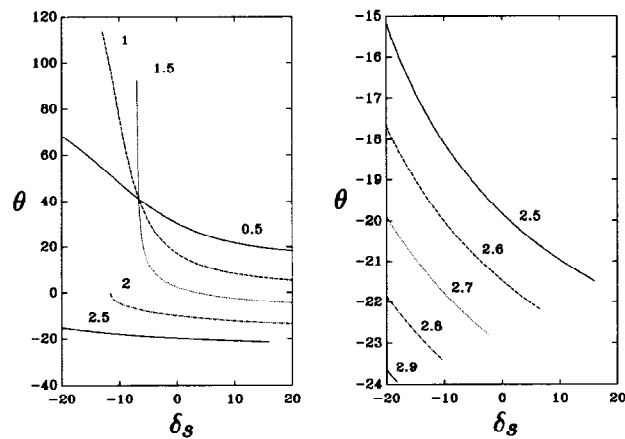


Fig. 10 Stable pitch angle solutions for variations in δB (in %W)

The metacentric height effect is shown in Fig. 11 where z_{GB} (in ft) is the parameter in the curves, and $\delta B = 2\%W$, $x_{GB} = -0.5\%L$, $\delta_b = 0$, $x_B = z_B = 0$. Although no qualitative changes in the form of the solutions are detected, increased z_{GB} strengthens motion stability, as expected.

Figure 12 depicts the effects of variations in the longitudinal center of buoyancy. The parameter x_B parametrizes the curves and is varied from +2 to -9% of vehicle length. For all curves $\delta_b = 0$, $\delta B = 2\%W$, $x_{GB} = -0.5\%L$, $z_{GB} = 0.1$ ft, and $z_B = 0$. The general trend shown in the figure is that positive values of x_B tend to produce stable solutions for positive dive plane angles. Similarly, negative values of x_B tend to have stable solutions for negative dive plane angles.

Finally, the effect of a nonzero bow plane angle δ_b is shown in Fig. 13. In this case, $\delta B = 2\%W$, $x_{GB} = -0.5\%L$, $z_{GB} = 0.1$ ft, and $x_B = z_B = 0$. The bow plane deflection is -20 deg. The significance of these results is the existence of two stable solutions over a range of δ_s . Following the discussion of the previous subsection, two more stable solutions exist, namely the supplementary solutions $(\theta, \phi) = (\pi - \bar{\theta}, \pi)$.

Simulation results

The previous stability analysis results are verified here by simulations using direct numerical integrations of the full six degrees-of-freedom equations of motion for the SDV. Simulations are performed for $\delta_b = 0$, $\delta B = 2\%W$, $x_{GB} = \pm 1\%L$, $z_{GB} = 0.1$ ft, $x_B = z_B = 0$, and $\delta_s = -15$ deg or -7 deg, so that direct comparison with the theoretical results of Figs. 1-8 is possible.

Figure 14 shows a plot of the pitch angle θ versus time t , for $x_{GB} = +1\%L$ and $\delta_s = -15$ deg. The dotted line marks the stable steady state solution from Fig. 5, and convergence of solutions to this value is observed. Similarly, a (θ, t) plot for $x_{GB} = -1\%L$ is shown in Fig. 15 where convergence to the steady state solution of Fig. 5 is observed. However, this steady state solution was found to be stable for the vertical plane only, see Fig. 6. The horizontal plane stability analysis of Fig. 7 indicated that this would be an unstable solution. The reason for this apparent contradiction in the results is attributed to the fact that the initial conditions for all horizontal plane variables p , ϕ , v , r were zero in the numerical integration. It is a natural consequence of the port/starboard symmetry of the equations of motion that this choice of initial conditions restricts motion in the vertical plane which is a subspace of the stable manifold of system (30) (Guckenheimer & Holmes 1983). Adding a small initial roll angle $\phi_0 = 1$ deg caused the vehicle to steady out at a different pitch angle as shown in Fig. 16. This initial roll angle also caused a nonzero steady state roll angle as shown in Fig. 17. In turn, this steady-state roll angle caused a nonzero steady state vehicle yaw rate and motion was not restricted in the vertical plane any longer. The vehicle experienced a steady state helical ascent to the surface (Booth 1977, McKinley 1991). Therefore, numerical integrations demonstrate a horizontal plane instability as predicted by the stability analysis.

This instability manifests itself as a divergent instability and is associated with the existence of a positive real solution of the generalized horizontal plane eigenvalue problem (54). Numerical experiments suggest a pitchfork bifurcation (Golubitsky & Schaeffer 1985) and this is the subject of current research. The results of Figs. 16 and 17 demonstrate also an extreme sensitivity of state trajectories to initial conditions. Small changes in the initial conditions appear to generate solutions with divergent characteristics even though the time histories appear to be identical for a large period of time before divergence occurs. Since numerical integrations can be carried out only for a limited time, the previous results show the need for a careful stability and bifurcation

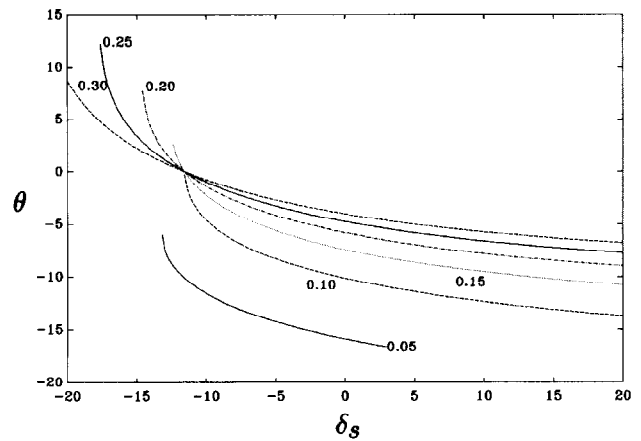


Fig. 11 Stable pitch angle solutions for variations in z_{GB} (in ft)

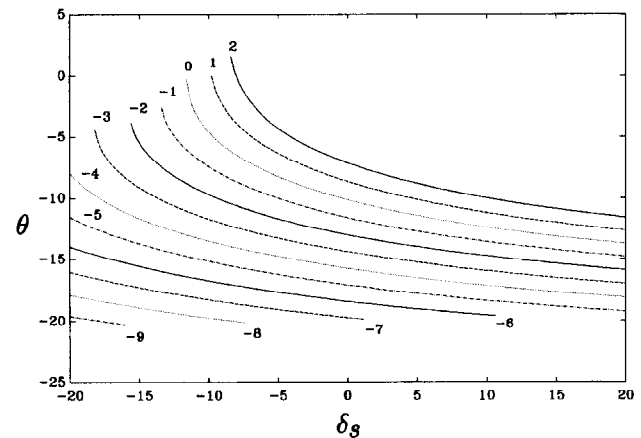


Fig. 12 Stable pitch angle solutions for variations in x_B (in %L)

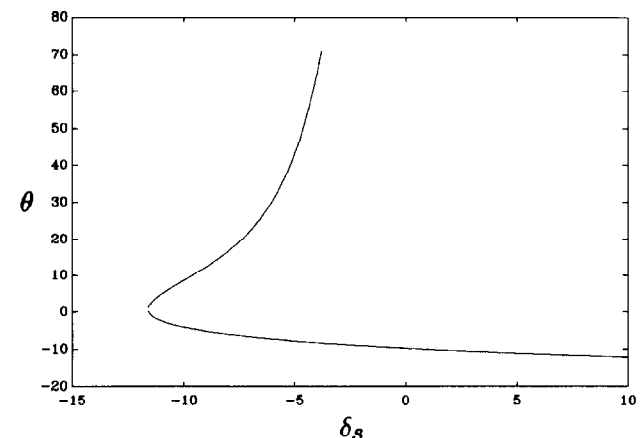


Fig. 13 Stable pitch angle solutions for bow plane angle $\delta_b = -20$ deg

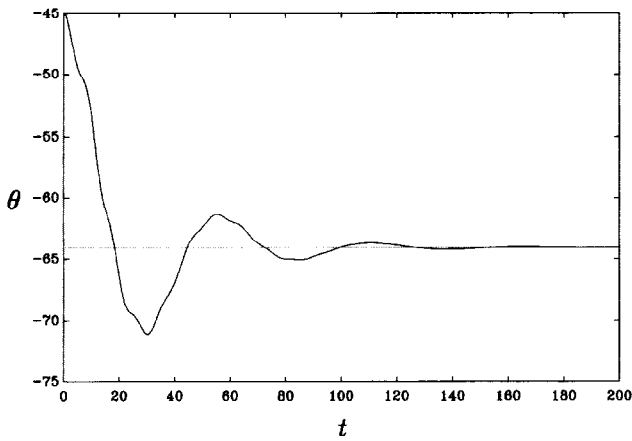


Fig. 14 Pitch response for $x_{GB} = +1\%L$ and $\delta_s = -15$ deg

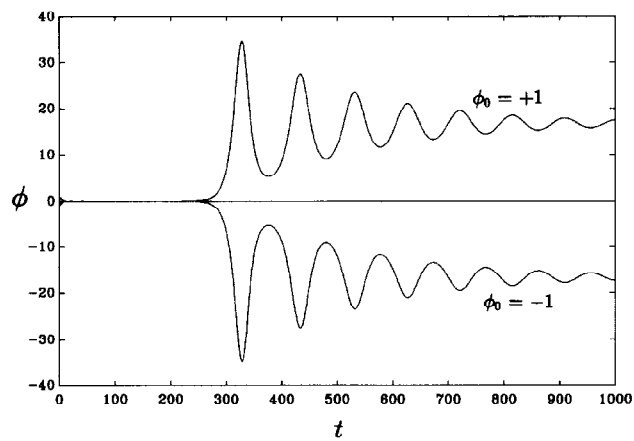


Fig. 17 Roll response for $x_{GB} = -1\%L$, $\delta_s = -15$ deg, and different initial roll angles ϕ_0 in deg

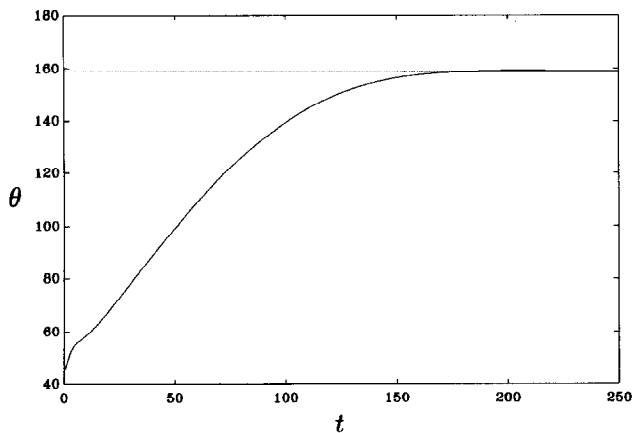


Fig. 15 Pitch response for $x_{GB} = -1\%L$, $\delta_s = -15$ deg, and zero initial roll angle ϕ_0

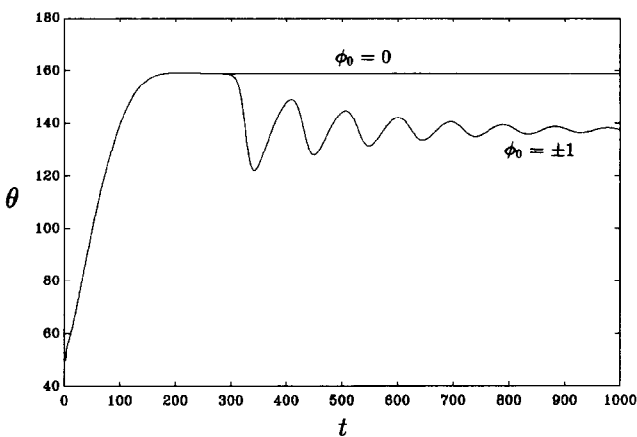


Fig. 16 Pitch response for $x_{GB} = -1\%L$, $\delta_s = -15$ deg, and different initial roll angles ϕ_0 in deg

analysis in order to establish local and global properties of solutions.

So far, the stability of the system has been assessed in the sense of Lyapunov. According to this, only an initial disturbance is given to the system in the form of initial conditions other than the system's equilibrium. It is natural to consider, however, that the vehicle will be under continuously acting disturbances arising from the environment, vortex shedding, and unmodeled dynamics. This brings the question of stability under permanently acting perturbations, in particular, stability of the inverted pendulum position under a random persistent disturbance in roll. It is known (Hahn 1967) that under continuously acting perturbations, the nominal point (31) of system (30) cannot be asymptotically stable any longer; however, a bounded persistent disturbance will result in a bounded motion in the neighborhood of the stable solution (31). This, of course, depends on the bounds of the disturbance.

In order to demonstrate stability under permanently acting perturbations, we consider the case $\delta_b = 0$, $\delta B = 2\%W$, $x_{GB} = -1\%L$, $z_{GB} = 0.1$ ft, $x_B = z_B = 0$, and $\delta_s = -7$ deg. According to Fig. 8 this results in a stable inverted pendulum configuration. A zero mean Gaussian noise was injected on the roll angle during simulations to simulate the effects of a continuously acting disturbance. This resulted in a random roll angle response with standard deviation of 5 deg. Two time histories in the pitch angle θ are presented in Fig. 18 with slightly different initial conditions θ_0 . It can be seen that the inverted pendulum stabilization persists depending on the initial conditions. The sensitivity of the system to the initial conditions is also evident from the results of the figure.

Finally, the results shown in Fig. 19 assess the response of the vehicle with identical initial conditions and different root-mean-square levels of random roll disturbance. The upper curve which shows the inverted pendulum stabilization was obtained with a roll standard deviation of 0.5 deg, while for the lower curve which shows stabilization to the supplementary pitch angle solution, the roll standard deviation was increased to 1 deg. Once more, the extreme sensitivity of solutions to random perturbations and the initial conditions is evident.

Decoupled roll and lateral motions

In order to get some physical interpretation of the counter-intuitive inverted pendulum stabilization discussed thus far,

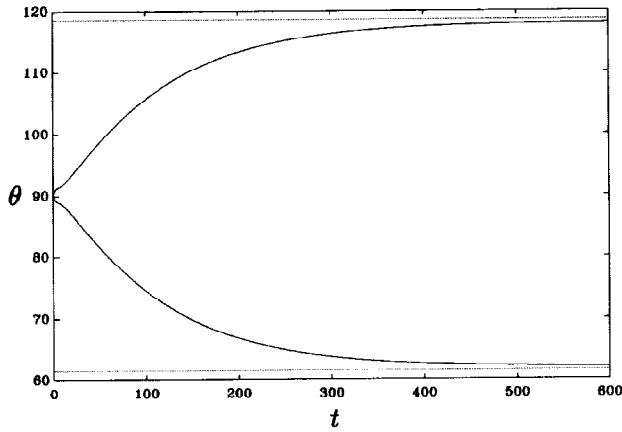


Fig. 18 Pitch response for $x_{GB} = -1\%L$, $\delta_s = -7$ deg, persistent roll disturbance and different initial conditions

consider the horizontal plane equations of motion and assume that there exists no dynamic coupling between roll and lateral dynamics in sway and yaw. The linearized (around $\phi = 0$) decoupled roll equation of motion then becomes

$$[\mathbf{B}_R][\dot{p}, \dot{\phi}]^T = [\mathbf{A}_R][p, \phi]^T \quad (55)$$

where

$$\mathbf{B}_R = \begin{bmatrix} I_x - K_p & 0 \\ 0 & 1 \end{bmatrix}$$

and

$$\mathbf{A}_R = \begin{bmatrix} K_p \bar{u} + (K_{wp} - mz_G) \bar{w} & -(z_G W - z_B B) \cos \bar{\theta} \\ 1 & 0 \end{bmatrix}$$

Similarly, the linearized decoupled sway/yaw equations of motion are

$$[\mathbf{B}_L][\dot{v}, \dot{r}]^T = [\mathbf{A}_L][v, r]^T \quad (56)$$

where

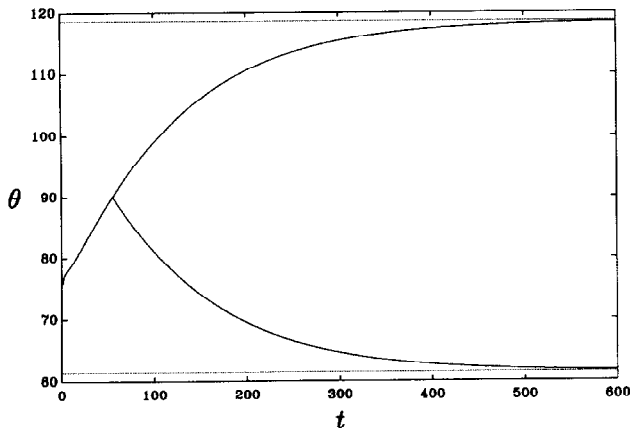


Fig. 19 Pitch response for $x_{GB} = -1\%L$, $\delta_s = -7$ deg, identical initial conditions, and different levels of persistent roll disturbance

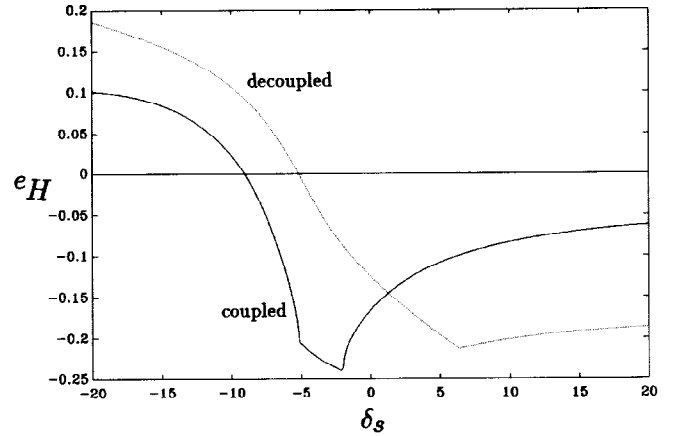


Fig. 20 Comparison of coupled and decoupled horizontal plane degree of stability

$$\mathbf{B}_L = \begin{bmatrix} m - Y_v & mx_G - Y_r \\ mx_G - N_v & I_z - N_r \end{bmatrix}$$

and

$\mathbf{A}_L =$

$$\begin{bmatrix} Y_v \bar{u} + Y_{vv} \bar{w} - C_{Dz} A_w |\bar{w}| & Y_{vr} \bar{w} + (Y_r - m) \bar{u} - C_{Dz} A_w x_A |\bar{w}| \\ N_v \bar{u} + N_{vv} \bar{w} - C_{Dz} A_w x_A |\bar{w}| & (N_r - mx_G) \bar{u} + N_{vr} \bar{w} - C_{Dz} I_A |\bar{w}| \end{bmatrix}$$

It can be seen that the eigenvalue problem (55) will always result in positive solutions if θ exceeds 90 deg. Studying roll motions decoupled from sway and yaw would, therefore, have missed the inverted pendulum stabilization possibility. A comparison of the degree of stability as predicted from the coupled problem (54) and from the decoupled problems (55) and (56) is shown in Fig. 20, for $x_{GB} = -1\%L$, $\delta_B = 2\%W$, $z_{GB} = 0.1$ ft, and $\delta_b = x_B = z_B = 0$. It can be seen that the dynamic coupling between roll and sway/yaw shifts the degree of stability curve to the left where, according to Fig. 5, solutions for θ greater than 90 deg occur.

As a final check, it should be pointed out that the hydrodynamic model used in this work has one major difference than a usual submarine model. Namely, the SDV possesses a keel instead of a sail, in order to house an extra propeller used for surface operations. As a result, the roll hydrodynamic coefficients K_v and $K_{\dot{v}}$ are positive, and K_{wp} is negative. For submarines the opposite is true, $K_v < 0$, $K_{\dot{v}} < 0$, and $K_{wp} > 0$. This sign change has no effect on the vertical plane steady state solutions but it does affect their horizontal plane stability indices. For this reason, we changed the signs of the above hydrodynamic coefficients so that they correspond to a vehicle with a sail instead of a keel. The result in terms of the horizontal plane stability index e_H is shown in Fig. 21, where it can be seen that despite the slight change in the values of e_H , the inverted pendulum stabilization persists.

Concluding remarks

The problem of steady-state response and dynamic stability analysis of submarines in free positive buoyancy ascent has been studied. The main parameters affecting response and stability were the stern and bow plane deflections, amount of excess buoyancy, and the relative positions of the centers

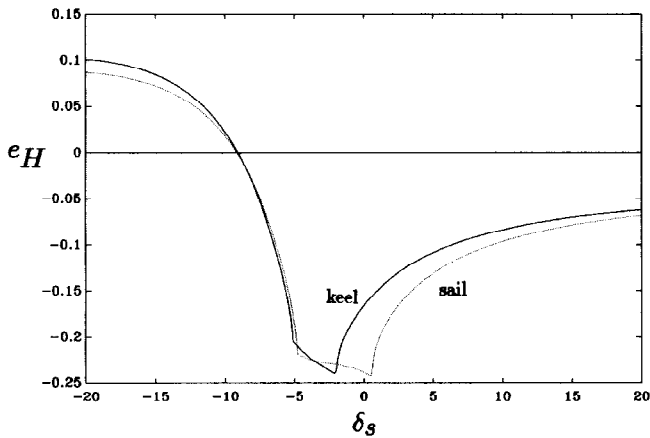


Fig. 21 Comparison of horizontal plane degree of stability for a vehicle with keel and sail

of gravity and buoyancy. The main conclusions of this work can be summarized as follows:

1. Steady-state motion is not, in general, restricted to the vertical plane unless the rudder is kept at zero, and the centers of gravity and buoyancy are located "symmetrically" with respect to the centerplane; i.e., $y_G W = y_B B$.

2. Four solutions in the vertical plane exist, some of them can be sometimes classified as nearly vertical ascents at relatively low speeds and large angles of attack, while others take the form of predominantly forward motions with high forward speeds and small angles of attack. Four solutions were identified with supplementary values for the pitch and roll angles, thus bringing the total number of steady-state vertical ascents to eight.

3. Motion stability was shown to naturally decouple into vertical plane (surge, heave, pitch) and horizontal plane (roll, sway, yaw) motions. The supplementary solutions were shown to have identical stability characteristics, and in general, two solutions were found to be stable.

4. Sensitivity analysis was performed with regards to important geometric parameters which demonstrated their effect on system response.

5. One stable solution was found to exhibit characteristics of an inverted pendulum. The vehicle was shown to be dynamically stable in this position, which is naturally statically unstable since it corresponds to a negative metacentric height.

6. This inverted pendulum stabilization was found to persist under continuously acting disturbances in roll. It was shown that the phenomenon can be attributed to the coupling between roll and sway/yaw motions.

7. Numerical integrations suggested an extreme sensitivity of the system to initial conditions and random disturbance levels. This sensitivity of solutions was found to occur for parameter ranges which allowed for the inverted pendulum stabilization to occur.

Work is continuing in the area to analyze the stability properties of all system solutions that are not restricted to the vertical plane. Bifurcation analysis is under current progress in order to classify the loss-of-stability cases and to establish boundaries of safe vehicle operations.

References

ABKOWITZ, M. 1969 *Stability and Motion Control of Ocean Vehicles*, MIT Press, Cambridge, Mass.

- BOOTH, T. B. 1977 Stability of buoyant underwater vehicles part I. predominantly forward motion. *International Shipbuilding Progress*, **24**, 279.
- BOOTH, T. B. 1977 Stability of buoyant underwater vehicles part II. near vertical ascent. *International Shipbuilding Progress*, **24**, 280.
- FALZARANO, J. M., SHAW, S. W., AND TROESCH, A. W. 1992 Application of global methods for analyzing dynamical systems to ship rolling motion and capsizing. *Journal of Bifurcation and Chaos*, **2**, 1.
- FELDMAN, J. 1979 DTNSRDC revised standard submarine equations of motion. Technical Report DTNSRDC-SPD-0393-09, David Taylor Research Center, Washington, D.C.
- FOSSEN, T. I. 1991 Nonlinear modelling and control of underwater vehicles. Dr. Ing. dissertation, Norwegian Institute of Technology, Trondheim.
- GERTLER, M. AND HAGEN, G. R. 1967 Standard equations of motion for submarine simulation. Technical Report DTMB 2510, David Taylor Research Center, Washington, D.C.
- GOLUBITSKY, M. AND SCHAEFFER, D. G. 1985 *Singularities and Groups in Bifurcation Theory I*, Springer-Verlag, New York.
- GUCKENHEIMER, J. AND HOLMES, P. 1983 *Nonlinear Oscillations, Dynamical Systems, and Bifurcations of Vector Fields*, Springer-Verlag, New York.
- HAHN, W. 1967 *Stability of Motion*, Springer-Verlag, New York.
- HUMPHREYS, D. E. 1989 The impact of speed varying hydrodynamic coefficients on UUV maneuvering performance. *Proceedings, 6th International Symposium on Unmanned Untethered Submersible Technology*, Durham, N. H.
- KANE, T. R., LIKINS, P. W., AND LEVINSON, D. A. 1983 *Spacecraft Dynamics*, McGraw-Hill, New York.
- MCKINLEY, B. D. 1991 Dynamic stability of positively buoyant submersibles: vertical plane solutions. Master's thesis, Department of Mechanical Engineering, Naval Postgraduate School, Monterey, Calif.
- SMITH, N. S., CRANE, J. W., AND SUMMEY, D. C. 1978 SDV simulator hydrodynamic coefficients. Report NCSC-TM231-78, Naval Coastal Systems Center, Panama City, Fla.
- TINKER, S. J. 1978 Fluid memory effects on the trajectory of a submersible. *International Shipbuilding Progress*, **25**, 290.

Appendix

The nonzero entries of the mass matrices M_V and M_H and the linearized system matrices A_V and A_H are given below. Variables u, w, θ are evaluated at equilibrium, the overbars have been dropped for convenience, and $\cos \phi = \pm 1$.

For the vertical plane

$$\mathbf{x}_v = [u, w, q, \theta]$$

we have

$$B_V(1,1) = m - X_w$$

$$B_V(1,3) = mz_G$$

$$B_V(2,2) = m - Z_w$$

$$B_V(2,3) = -(Z_q + mx_G)$$

$$B_V(3,1) = mz_G$$

$$B_V(3,2) = -(M_w + mx_G)$$

$$B_V(3,3) = I_y - M_q$$

$$B_V(4,4) = 1$$

and

$$A_V(1,1) = -2uC_{D0} + w(X_{w\delta_s}\delta_s + X_{w\delta_b}\delta_b) + 2u(X_{\delta_s\delta_s}\delta_s^2 + X_{\delta_b\delta_b}\delta_b^2)$$

$$A_V(1,2) = 2X_{uw}w + u(X_{w\delta_s}\delta_s + X_{w\delta_b}\delta_b)$$

$$A_V(1,3) = w(X_{wq} - m) + u(X_{q\delta_s}\delta_s + X_{q\delta_b}\delta_b)$$

$$A_V(1,4) = -(W - B) \cos \theta$$

$$A_V(2,1) = Z_w w + 2u(Z_{\delta_s}\delta_s + Z_{\delta_b}\delta_b)$$

$$A_V(2,2) = Z_w u - 2C_{Dz}A_w|w|$$

$$A_V(2,3) = u(Z_q + m) + 2C_{Dz}A_w x_A|w|$$

$$A_V(2,4) = -(W - B) \sin \theta \cos \phi$$

$$A_V(3,1) = M_w w + 2u(M_{\delta_s}\delta_s + M_{\delta_b}\delta_b)$$

$$\begin{aligned}
A_V(3,2) &= M_w u + 2C_{Dz} A_w x_A |w| \\
A_V(3,3) &= (M_q - mx_G) u - mz_G w - 2C_{Dz} I_A |w| \\
A_V(3,4) &= (x_G W - x_B B) \sin \theta \cos \phi - (z_G W - z_B B) \cos \theta \\
A_V(4,3) &= \cos \phi
\end{aligned}$$

where

$$I_A = \int x^2 b(x) dx$$

For the horizontal plane

$$\mathbf{x}_H = [p, \phi, v, r]$$

we have

$$\begin{aligned}
B_H(1,1) &= I_x - K_p \\
B_H(1,3) &= -(K_v + mz_G) \\
B_H(1,4) &= -K_r \\
B_H(2,2) &= 1 \\
B_H(3,1) &= -(Y_p + mz_G) \\
B_H(3,3) &= m - Y_v \\
B_H(3,4) &= mx_G - Y_r
\end{aligned}$$

$$\begin{aligned}
B_H(4,1) &= -N_p \\
B_H(4,3) &= mx_G - N_v \\
B_H(4,4) &= I_z - N_r
\end{aligned}$$

and

$$\begin{aligned}
A_H(1,1) &= K_p u + (K_{wp} - mz_G) w \\
A_H(1,2) &= -(z_G W - z_B B) \cos \theta \cos \phi \\
A_H(1,3) &= K_v u + K_{vw} w \\
A_H(1,4) &= u(K_r + mz_G) + K_{wr} w \\
A_H(2,1) &= 1 \\
A_H(2,4) &= \tan \theta \cos \phi \\
A_H(3,1) &= Y_p u + (Y_{wp} + m) w \\
A_H(3,2) &= (W - B) \cos \theta \cos \phi \\
A_H(3,3) &= Y_v u + Y_{vw} w - C_{Dz} A_w x_A |w| \\
A_H(3,4) &= Y_{wr} w + (Y_r - m) u - C_{Dz} A_w x_A |w| \\
A_H(4,1) &= mx_G w + N_p u + N_{wp} w \\
A_H(4,2) &= (x_G W - x_B B) \cos \theta \cos \phi \\
A_H(4,3) &= N_v u + N_{vw} w - C_{Dz} A_w x_A |w| \\
A_H(4,4) &= u(N_r - mx_G) + N_{wr} w - C_{Dz} I_A |w|
\end{aligned}$$